Aerodynamic and aeroacoustic wind tunnel tests of a half wing model with a full-span droop-nose leading edge

Seiji Adachi, Karlheinz Bay, Peter Brandstätt, Wolfgang Herget and John C. Simpson
Fraunhofer Institute for Building Physics, 70569 Stuttgart, Germany, Email: seiji.adachi@ibp.fraunhofer.de

Introduction

The next-generation low-noise high-lift devices is one of mainstream technologies targeted in the Low Noise Configuration (LNC) domain of the Clean Sky Green Regional Aircraft (GRA) project [1]. The Fraunhofer Institute contributes to development of this technology by proposing a droop-nose leading edge (LE) that would in near future succeed the conventional LE devices such as slats and Krueger flaps. In our computational fluid dynamics (CFD) and computational aeroacoustics (CAA) analysis [2], good aerodynamic and aeroacoustic performance of this model has already been predicted. The purpose of this study is to experimentally confirm the performance in wind tunnel tests using a 1:6-scaled half wing model [3]. This paper reports the procedure and results of these tests by comparing with those predicted in CFD and CAA analysis.

Droop-Nose Leading Edge

A three dimensional setting of the droop-nose leading edge as examined in our tests, is shown in Fig. 1. This leading edge configuration is drooped almost along the entire span from the root to the tip of the wing; complimenting the high lift flaps setting at the trailing edge. This is a promising wing configuration, providing ample high-lift performance with low noise cost for the final GRA-LNC program development phase.

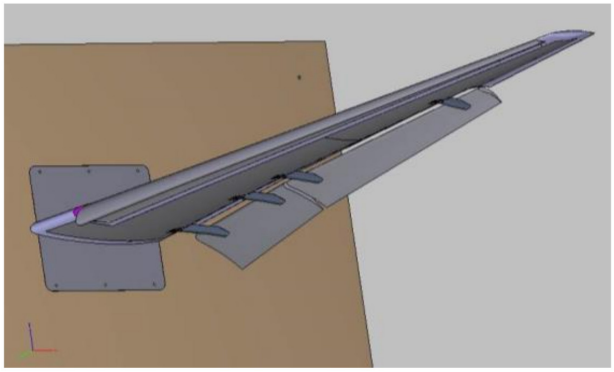

Figure 1: The full-span droop-nose leading edge proposed in this study. The leading edge is drooped almost entirely along the span, i.e., from 18% to 98% span.

Review of CFD and CAA Analysis

CFD and CAA analysis has been done in the full-scale condition to predict the performance of the model before the wind tunnel tests. The lift coefficients [†] c_l resulted in this analysis is shown in Fig. 2. The model can be set in three different configurations: (1) clean wing that has no deployed flaps or droop-nose, (2) high-lift baseline that has deployed flaps but has no droop-nose and (3) high-lift droop-nose configuration meaning to have both deployed flaps and a (nearly full-span) droop-nose leading edge. As shown in Fig. 2, the c_l of the clean wing configuration is gradually increasing up to 1.5 as the angle of attack α is increased up to 16 degrees. The high lift baseline has much larger c_l than that of the clean wing when α is small. This configuration, however, gets a stall immediately after α becomes greater than 6 degrees. This is not acceptable as a high-lift configuration. This disadvantage can be successfully resolved with the droop-nose configuration: The c_l can again keep increasing up to the angle of 15 degrees.

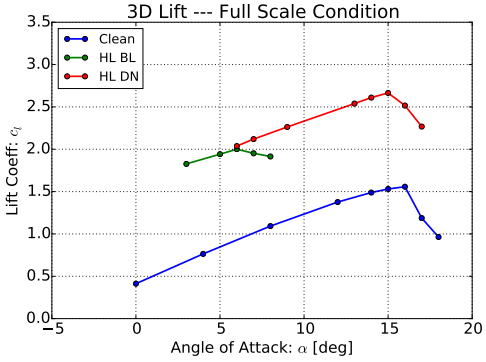

Figure 2: Lift coefficients of three different wing configurations: (1) clean wing, (2) high-lift baseline and (3) high-lift droop-nose, estimated in CFD analysis in the full-scale condition.

Noise radiation patterns estimated in our CAA analysis are presented in Fig. 3. The left picture shows the patterns of high-lift baseline and the right one does those of droop-nose configurations. In each configuration, blue and green circles are the patterns just before and after a stall, respectively. By comparing both configurations, we find no significant difference in the radiation patterns, especially in the forward direction which may be due to noise radiated from the leading edge. Namely, no penalty in terms of aeroacoustic performance could be found due to the droop-nose configuration. In each configuration, the noise level is, however, about 2 dB higher after a stall than before a stall. This implies that the analysis cap-

[†]Here by c_l we mean the 3D integrated lift coefficients. They are not the usual 2D coefficients of these.

tures a general tendency of increasing aeroacoustic noise when a stall occurs. This warrants the physical basis of the CAA analysis to a certain extent.

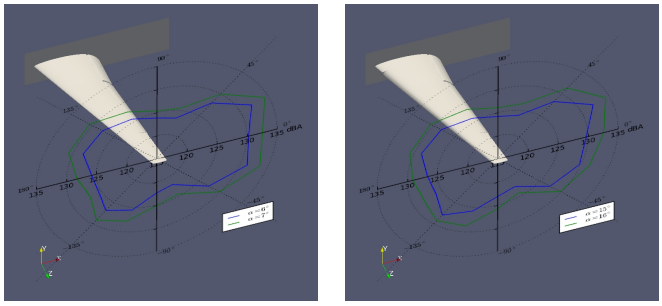

Figure 3: Noise radiation patterns of the high-lift baseline (left) and droop-nose (right) configurations estimated in CAA analysis.

Wind Tunnel Test Procedure

An automotive wind tunnel was hired for the test. This tunnel is primarily an aerodynamic wind tunnel. Far-field noise spectra of the wing model would therefore be somewhat contaminated by the wind tunnel background noise. However, some aeroacoustic measurement was still possible such as noise source detection using a beamforming system.

Figure 4 shows three different configurations of the 1:6-scaled wing model: clean wing, high-lift baseline and droop-nose. One can clearly see that the flaps are deployed in the two high-lift configurations, whereas they are retracted in the clean configuration. It is also manifest that the clean wing and high-lift baseline configurations have an original undrooped leading edge.

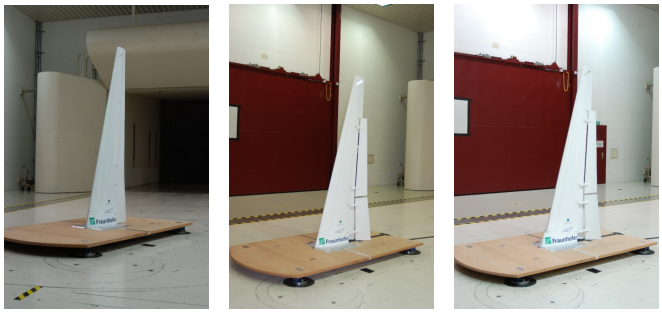

Figure 4: The wing model in three wing configurations: clean wing (left), high-lift baseline (middle) and high-lift droop-nose (right). The model is mounted on a wooden platform and installed in the wind tunnel.

A turbulator or transition tripping device [4] shown in Fig. 5 was also tested. The device can compensate the small Reynolds number effect in a scaled condition. For this purpose, a metal rod of 1.5 mm diameter was just stuck with an aluminum tape on the upper side of the wing near the leading edge.

The entire measurement setup is shown in Fig. 6. In addition to measuring lift and drag of the wing using

Figure 5: Turbulator or a transition tripping device.

a balance equipped under the floor, we examined sound source locations with a beamforming system, mechanical vibration with a laser vibrometer and far-field noise using microphones outside of the flow. The overall test procedure was also monitored with video cameras.

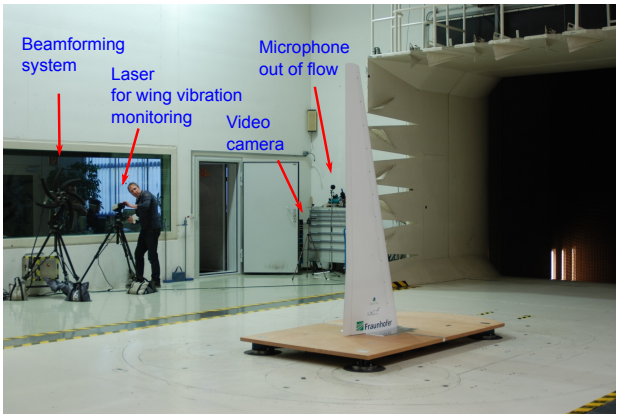

Figure 6: Overview of the test setup.

Wind Tunnel Test Results

Aerodynamic performance

Measured lift coefficients c_l of the wing with and without the turbulator are presented in Figs. 7 (a) and (b), respectively. Estimated coefficients c_l in CFD analysis in the same 1:6-scaled condition (lower) are also presented in Fig. 7 (c). Due to the Reynolds number effect [5], the resulted c_l is different from c_l in Fig. 2 estimated in the full-scale condition. Figures 7 (a) and (c) look very similar: The CFD analysis reasonably predicts the overall magnitude of c_l, the max lift coefficients $c_{l_{max}}$ and the stall angles of these configurations. This implies, however, that the turbulator did not work very well.

In the case without the turbulator, the c_l of the droop-nose configuration keeps increasing up to 2.5 as the angle of attack α goes up to 20 degrees. This is an extraordinary result that can not be accepted immediately. Deeper inspection of this result is needed in future. In the other configurations, a good agreement between the experiment and CFD analysis was achieved.

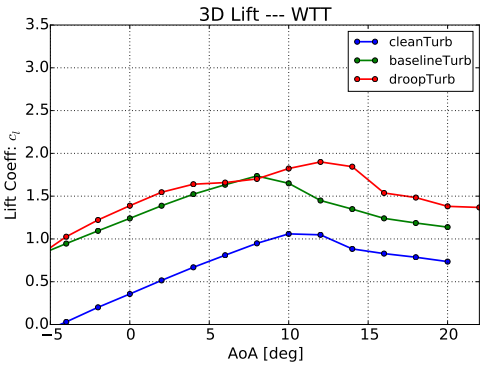

(a) Measured c_l of the cases with the turbulator.

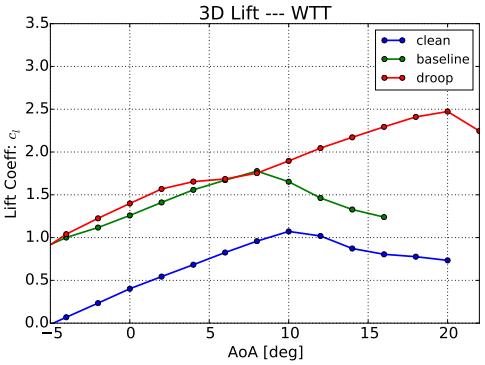

(b) Measured c_l of the cases without the turbulator.

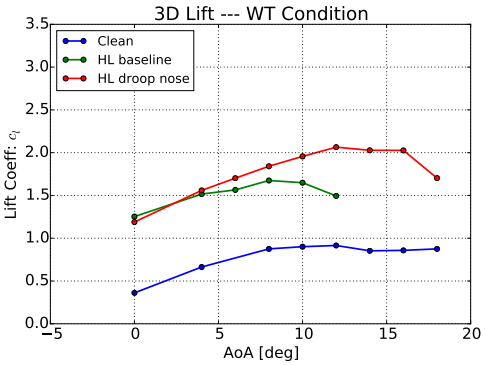

(c) Estimated c_l in CFD analysis in the same scaled condition.

Figure 7: Measured lift coefficients of the wing model (a) with and (b) without the turbulator and (c) those estimated in CFD in the same 1:6-scaled condition for comparison.

Noise source detection in a beamforming system

The results of noise source detection using a beamforming system [6] are listed in Table 1. Detected noise sources are marked with a cross for three different wing configurations, for two angles of attack and for various frequency bands. No salient noise sources were detected in the clean wing configuration. Some vindicative sources were detected in the high-lift configurations.

Figure 8 shows the overall sound pressure levels of these wing configurations with and without the turbulator. All the cases have a general tendency of the noise level increasing as the angle of attack is increased from 0 to 16 degrees. However, no systematic tendency in level difference among the cases could be found. The difference is therefore considered to be within the measurement error range.

Table 1: Sound source detected in an acoustic beamforming system in the 1/3-octave bands for three different wing configurations: clean wing, high-lift droop-nose without and with a transition tripping device (turbulator) and for two different angles of attack: 0 and 12 degrees. The x means that a noise source is detected.

Wing Config.	α[°]	1/3-octave [Hz] 630	800	1000	1250	1600	2000	2500
Clean wing	0	-	-	-	-	-	-	-
	12	-	-	-	-	-	-	-
HL-DN	0	-	x	-	-	-	-	x
	12	-	x	-	-	-	-	x
HL-DN-TB	0	-	x	-	-	-	-	x
	12	-	x	-	-	-	-	x

		1/3-octave [Hz] 3150	4000	5000	6300	8000	10000
Clean wing	0	-	-	-	-	-	-
	12	-	-	-	-	-	-
HL-DN	0	x	x	x	x	-	-
	12	x	x	x	x	x	x
HL-DN-TB	0	x	x	x	x	x	x
	12	x	x	x	x	x	x

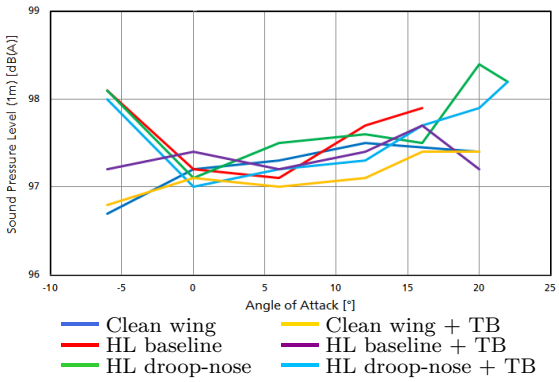

Figure 8: Overall sound pressure levels of three different wing configurations as functions of the angle of attack α.

Beamforming camera view examples are shown in Fig. 9. Mostly, noise sources were detected at the leading edge, at the flaps and at the stay connecting the flap to the wing main part. From camera views, we could not find any qualitative difference between the high-lift baseline and droop-nose configurations.

Far-field noise analysis

By using two microphones placed outside of the flow on the upper and lower sides of the wing, acoustic signals were measured. The signals cannot be regarded as being free from background noise. Nevertheless, the signals were analyzed as a scoping effort. Spectra shown in Fig. 10 are for the cases of (a) no wing model installed in the tunnel, (b) the clean wing, (c) high-lift baseline and (d) high-lift droop-nose configurations, respectively.

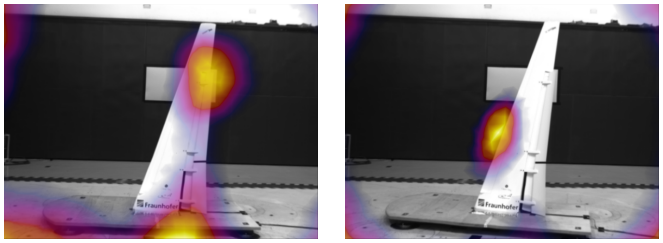

Figure 9: Beamforming camera views of detected noise sources.

The angle of attack was 20 degrees in all the cases. A consistent level difference between the two microphones in a frequency range from 50 to 100 Hz was found in all these cases. This is probably due to acoustic characteristics of the wind tunnel test section. Other than that, the analysis did not delve into the difference among the wing configurations.

In Fig. 10 (e), the spectrum of the high-lift droop-nose configuration (solid lines) is compared with that of the case where no wing model is installed (dashed lines). Below 500 Hz, it is difficult to find a meaningful difference in these spectra. Both the solid and dashed lines fit together in the low frequency region. Only the difference due to microphone positions shown in red and green exists. This implies that noise spectra of the wing are masked with the background noise. Above 500 Hz, however, the level of the high-lift droop-nose wing is about 1 to 5 dB higher. This is an indication of noise generated by the wing model.

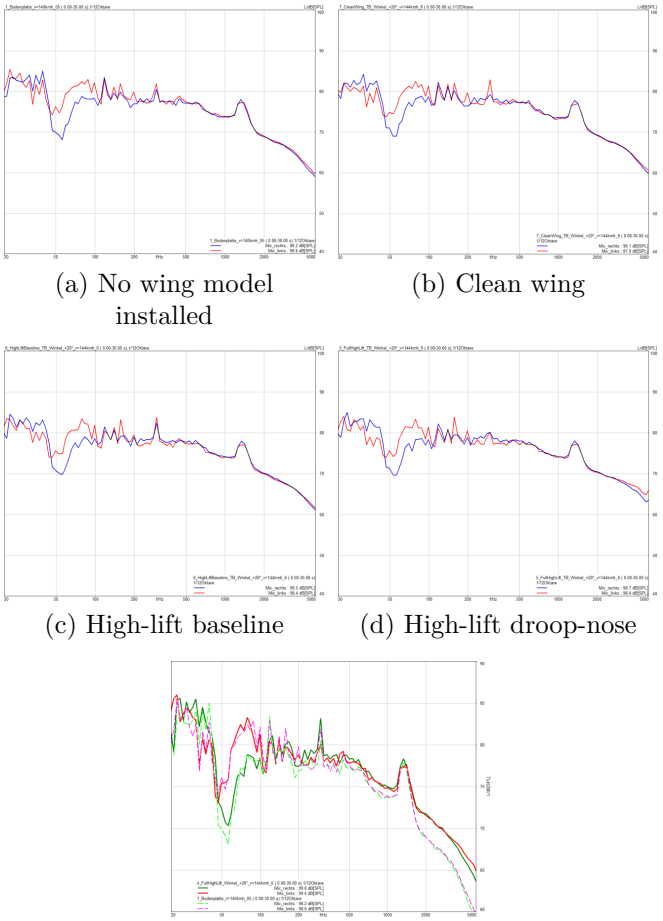

(a) No wing model installed (b) Clean wing

(c) High-lift baseline (d) High-lift droop-nose

(e) Comparison

Figure 10: Spectra of the microphone signals for the cases of (a) no wing model installed in the tunnel, (b) clean wing, (c) high-lift baseline and (d) high-lift droop-nose configurations, respectively. Cases (a) and (d) are compared in (e).

Summary

The following three points are addressed as a summary:

1. In the aerodynamic analysis, the droop-nose configuration shows an extraordinary result: very high maximum lift coefficient $c_{l\max}$ at a large stall angle α_{stall}. This should however be more confirmed in future.

2. In the other configurations, good agreement between CFD analysis and wind tunnel tests was found. This provides more evidence to believe CFD analysis results both in scaled and full-scale conditions. In other words, a good aerodynamic performance of the droop-nose leading edge found in full-scale analysis is more probable.

3. No aeroacoustic penalty of the droop-nose wing configuration was found both in CAA analysis and wind tunnel tests. This is a good news for the further development of the droop-nose leading edge.

Acknowledgments

This research is funded by the European Commission in the Seventh Framework Programme (FP7/2007-2013) for the Clean Sky Joint Technology Initiative under the grant agreement No. CSJU-GAM-GRA-2008-001.

References

[1] Clean Sky Green Regional Aircraft (GRA) project, URL:
`http://www.cleansky.eu/green-regional-aircraft-gra`

[2] New (full-span) Droop Nose design and CFD/CAA assessment (Output O2.3.1-12) GRA-2.3.1-TN-FhG-TECH-214596 A.

[3] Wing High-Lift WT Model with Droop Nose & T/E Flap – Hardware (Deliverable D2.3.1-9) GRA-2.3.1-DL-FhG-TECH-215633 A.

[4] Barlow, J.B., Rae Jr., W.H. & Pope, A. (1999). Low-Speed Wind Tunnel Testing, 3rd Ed. *Wiley* New York, chap. 8.2.

[5] Barlow, J.B., Rae Jr., W.H. & Pope, A. *op. cit.*, chap. 8.

[6] HEAD VISOR System, URL:
`https://www.head-acoustics.de/eng/nvh_head-visor.htm`